ELSEVIER

Journal of Applied Geophysics 50 (2002) 3–19

JOURNAL OF APPLIED GEOPHYSICS

www.elsevier.com/locate/jappgeo

A review of the basic principles for proton magnetic resonance sounding measurements

Anatoly Legchenko [a,*], Pierre Valla [b]

[a] BRGM, BP 6009, 45060 Orléans Cedex, France
[b] IRIS-Instruments, BP 6007, 45060 Orléans Cedex, France

Abstract

In the last two decades, proton magnetic resonance has emerged as a new geophysical technique allowing direct, noninvasive groundwater investigations from the surface. The theoretical basis and appropriate numerical modelling schemes are presented together with the data acquisition, signal processing, and interpretation aspects. Examples are given with both synthetic and field data. The current state-of-the-art method corresponds to one-dimensional application of the technique and this already offers quite numerous possibilities of application for hydrogeological investigations. © 2002 Elsevier Science B.V. All rights reserved.

Keywords: Proton magnetic resonance; Numerical modelling schemes; Hydrogeological investigations

1. Introduction

The purpose of this article is to give an overview of the various aspects of proton magnetic resonance sounding of the subsurface, namely, the physical principles, numerical modelling, data acquisition, data processing, and interpretation. The current state-of-the-art method is the result of the developments that Russian scientists have been conducting for two decades, complemented since 1994 with the co-operation of the French geological survey (BRGM) and IRIS-Instruments.

2. Magnetic resonance for protons

The detailed understanding of magnetic resonance entails using quantum spin physics description at the atomic scale and Boltzmann statistics to obtain the macroscopic effects, leading to the Heisenberg equation (Abragam, 1961). We will focus on the basic phenomena here. The starting point is the spin property of atom components (electron, proton, neutron); when such a component has a nonzero spin, it behaves like a tiny magnet and its spin vector (or magnetisation vector) aligns itself with the ambient static magnetic induction field $\boldsymbol{B}_0$. The energy configurations or states are discrete, the lowest energy is obtained when the magnetisation vector is parallel to the static field, and the highest energy when it is antiparallel. Individual unpaired electrons, protons, and neutrons each possesses a spin of 1/2, and the two previous states are the only possible ones. The corresponding energy diagram is depicted in Fig. 1.

The transition from one state to the other occurs through the absorption or emission of a photon whose energy matches the energy difference between the two states. The energy E of a photon is related to its frequency f: $E=\hbar\omega=2\pi\hbar f$, where $\hbar$ is Planck's cons-

* Corresponding author.
E-mail addresses: a.legtchenko@exchange.brgm.fr (A. Legchenko), pierre.valla@mines.org (P. Valla).

0926-9851/02/$ - see front matter
PII: S0926-9851(02)00127-1

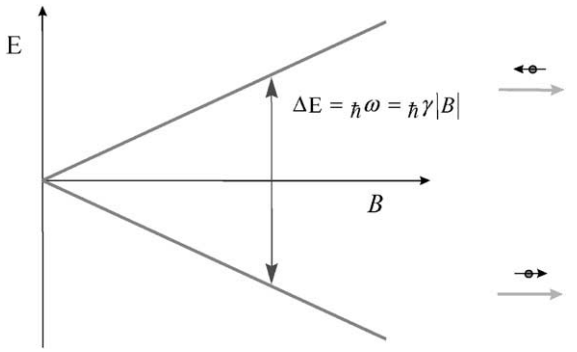

Fig. 1. Energy diagram for spin 1/2 with two states.

tant: $\hbar = 6.626 \cdot 10^{-34}/2\pi$ [J/rad]. The match occurs at the Larmor frequency f_0 defined by the relationship: $\omega_0 = 2\pi \cdot f_0 = \gamma \cdot |\boldsymbol{B}_0|$, where γ is the gyromagnetic ratio. For hydrogen protons in water molecules,

$$\gamma = 2\pi \cdot 4.254597 \cdot 10^{-2} = 0.2675 \text{ [rad/s/nT]}. \quad (1)$$

Two types of quantum interaction occur between a spin of 1/2 proton and a matching photon (Fig. 2):

- when the proton is in the low-energy state, it may absorb the photon and jump to the high-energy state;
- when the proton is in the high-energy state, it may emit a second photon under the induced effect of the incoming one and jump back to the low-energy state.

Under a nonzero static magnetic field, there is a slight unbalance of the proton's spin orientation because the parallel low-energy state is slightly more numerous according to Boltzmann's law. When a matching frequency electromagnetic wave is superimposed, a cyclical behaviour is observed depending on the intensity and duration of the photons flux sent over the protons, as a result of the two antagonistic quantum interactions: at first, the antiparallel high-energy population increases, then it reaches a maximum with a reverse unbalance compared to the static equilibrium, and if the photons flux continues, it decreases back to the starting point before increasing again and so on.

From the macroscopic point of view, the magnetic resonance phenomenon is described by the Bloch equations (Abragam, 1961; Slichter, 1990). These equations are usually written in a coordinate system where the z-axis unit vector u_z is aligned along the static magnetic induction field $\boldsymbol{B}_0 = \mu \boldsymbol{H}_0$. The key role is played by the energising magnetic induction field $\boldsymbol{B}^{\mathrm{Tx}}$ at the Larmor frequency f_0. The Bloch equations describe the behaviour of the magnetisation vector $\boldsymbol{M}$, linked to the spin property of the protons when

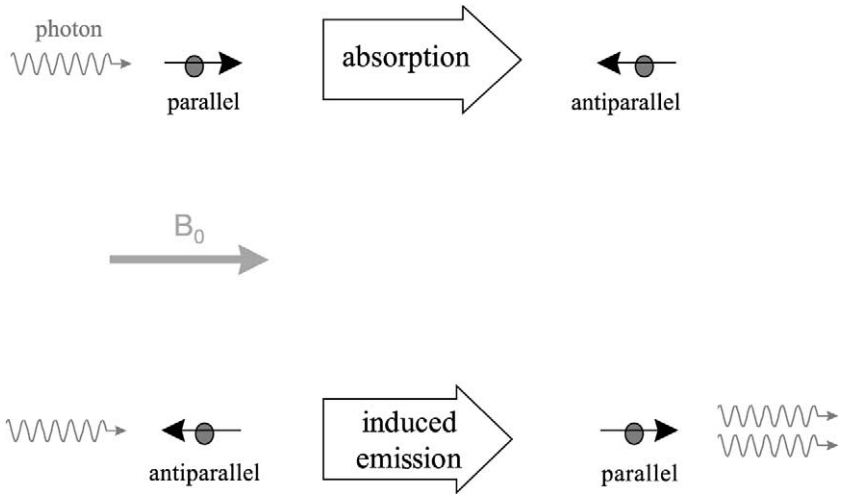

Fig. 2. Transition from one energy state to the other through matching photon absorption or induced emission.

subjected to the total induction field $\boldsymbol{B}=\boldsymbol{B}_0+\boldsymbol{B}^{\mathrm{Tx}}$, assuming that the magnitude of $\boldsymbol{B}^{\mathrm{Tx}}$ is small compared to that of $\boldsymbol{B}_0$, viz.:

$$\frac{\mathrm{d}M_z}{\mathrm{d}t}=\gamma(\boldsymbol{M}\times\boldsymbol{B})_z+\frac{M_0-M_z}{T_1}$$
$$\text{and}\quad \frac{\mathrm{d}M_{x,y}}{\mathrm{d}t}=\gamma(\boldsymbol{M}\times\boldsymbol{B})_{x,y}-\frac{M_{x,y}}{T_2} \tag{2}$$

where M_0 is the nuclear magnetisation for protons in water at thermal equilibrium, T_1 and T_2 are the time constants of the longitudinal and transversal relaxation. M_0 is described by the Curie equation:

$$M_0=N\cdot B_0\frac{\gamma^2\cdot\hbar^2}{4kT}=\chi_0\cdot H_0 \tag{3}$$

where N is the number of hydrogen protons per unit volume, T is the absolute temperature, $\hbar$ is the previously defined Planck's constant, and the Boltzmann's constant is $k=1.3805\cdot10^{-23}$ [J/°].

Since $N=6.692\cdot10^{28}$ [/m^3], it is found that $M_0=3.287\cdot10^{-3}B_0$ at 293 K (20 °C) and $M_0=3.403\cdot10^{-3}B_0$ at 283 K (10 °C). We will take this latter value in the following, which corresponds to a nuclear paramagnetic susceptibility for protons in water $\chi_0=4.276\cdot10^{-9}$ [SI units].

If we use a frame of reference x'–y' rotating around the z-axis (Fig. 3) with a clockwise rotation at angular frequency, the Bloch equations simplify to:

$$\frac{\mathrm{d}M_z}{\mathrm{d}t}=\gamma(\boldsymbol{M}\times\boldsymbol{B}^{\mathrm{Tx}})_z+\frac{M_0-M_z}{T_1}$$
$$\text{and}\quad \frac{\mathrm{d}M_{x',y'}}{\mathrm{d}t}=\gamma(\boldsymbol{M}\times\boldsymbol{B}^{\mathrm{Tx}})_{x',y'}-\frac{M_{x',y'}}{T_2} \tag{4}$$

If the energising induction field $\boldsymbol{B}^{\mathrm{Tx}}$ is applied starting when the magnetisation vector is at equilibrium, $\boldsymbol{M}=M_0u_z$, its only effective part is that transverse to $\boldsymbol{B}_0$, namely:

$$\boldsymbol{B}_\perp^{\mathrm{Tx}}=u_z\times(\boldsymbol{B}^{\mathrm{Tx}}\times u_z)=B_\perp^{\mathrm{Tx}}\cdot\cos(\omega_0t)\cdot u_\perp^0$$
$$=B_\perp^{\mathrm{Tx}}\cdot\frac{1}{2}(u_\perp+u_\perp^-) \tag{5}$$

where $u_\perp$ is a unit vector rotating clockwise at angular frequency ω_0 around u_z (Fig. 3c) and $u_\perp^-$ a unit vector rotating counterclockwise and given by

$$u_\perp=\cos(\omega_0t)\cdot u_\perp^0+\sin(\omega_0t)\cdot u_\perp^0\times u_z \tag{6a}$$

$$u_\perp^-=\cos(\omega_0t)\cdot u_\perp^0-\sin(\omega_0t)\cdot u_\perp^0\times u_z \tag{6b}$$

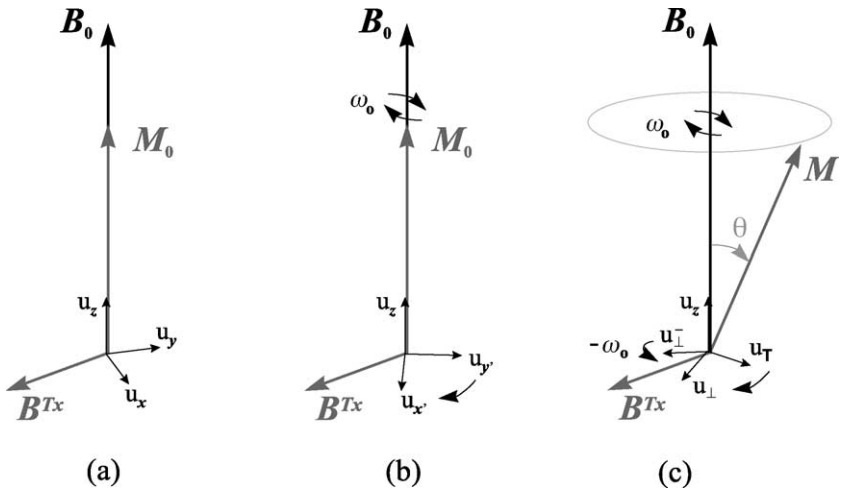

Fig. 3. The (a) fixed and (b) rotating frames of reference, and (c) tilting of the magnetisation vector.

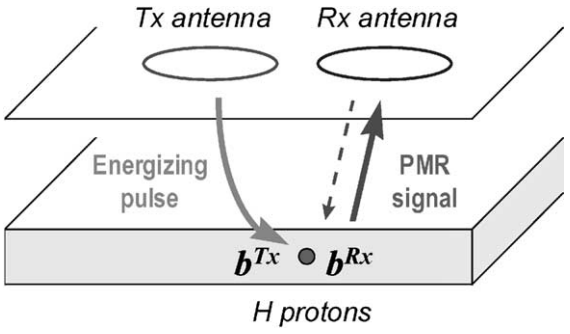

Fig. 4. Schematics of proton magnetic resonance measurement array.

In the above equations, $B_{\perp}^{\mathrm{Tx}}$ is constant since the time-dependence is now localised in the frame rotation. As the Bloch equations will be integrated for energising pulses which are quite many (a few tens) long Larmor periods, only the clockwise rotating components produce a nonzero time-averaged torque on the magnetisation of the protons. Hence, $\boldsymbol{B}^{\mathrm{Tx}}$ can be replaced by $1/2B_{\perp}^{\mathrm{Tx}}u_{\perp}$ in Eq. (4) leading to:

$$\frac{\mathrm{d}M_z}{\mathrm{d}t} = -\gamma \cdot M_{\top}\left(\frac{1}{2}B_{\perp}^{\mathrm{Tx}}\right) + \frac{M_0 - M_z}{T_1}$$

$$\text{and} \quad \frac{\mathrm{d}M_{\top}}{\mathrm{d}t} = \gamma \cdot M_z\left(\frac{1}{2}B_{\perp}^{\mathrm{Tx}}\right) - \frac{M_{\top}}{T_2} \tag{7}$$

where $u_{\top} = u_z \times u_{\perp}$. If $\boldsymbol{B}^{\mathrm{Tx}}$ is a pulse of duration τ (short enough, compared to T_1 and T_2 so that the decay may be neglected) before $t=0$, the solution of Eq. (7) can be approximated as:

$$M_z(t)\,|_{-\tau\le t\le 0} = M_0 \cdot \cos\left(\frac{1}{2}\gamma \int_{-\tau}^{t} B_{\perp}^{\mathrm{Tx}} \cdot \mathrm{d}t\right) \tag{8a}$$

$$M_{\top}(t)\,|_{-\tau\le t\le 0} = M_0 \cdot \sin\left(\frac{1}{2}\gamma \cdot \int_{-\tau}^{t} B_{\perp}^{\mathrm{Tx}}\mathrm{d}t\right) \tag{8b}$$

$$M_z(t)\,|_{\tau\ge 0} = M_0 \cdot \left[1 - \left(1 - \cos\left(\frac{1}{2}\gamma \cdot \int_{-\tau}^{0} B_{\perp}^{\mathrm{Tx}}\mathrm{d}t\right)\right) \cdot e^{-t/T_1}\right] \tag{8c}$$

$$M_{\top}(t)\,|_{\tau\ge 0} = M_0 \cdot \sin\left(\frac{1}{2}\gamma \int_{-\tau}^{0} B_{\perp}^{\mathrm{Tx}} \cdot \mathrm{d}t\right) \cdot e^{-t/T_2} \tag{8d}$$

This corresponds to a tilting of the magnetisation vector from the z-axis (Fig. 3c) by an angle θ given by

$$\theta = \frac{1}{2}\gamma \cdot \int_{-\tau}^{0} B_{\perp}^{\mathrm{Tx}}\mathrm{d}t = \frac{1}{2}\gamma \cdot B_{\perp}^{\mathrm{Tx}} \cdot \tau \tag{9}$$

followed by relaxation decay towards the static equilibrium.

Since $(u_{\perp}, u_{\top}, u_z)$ is a right-handed frame rotating clockwise around u_z at an angular frequency ω_0 in a fixed frame of reference, the transverse component $M_{\top}$ of the magnetisation vector behaves as the sum of two orthogonal dipoles with a 90° phase difference, i.e.

$$\begin{aligned} M_{\top}u_{\top} &= M_{\top} \cdot (\cos(\omega_0 t) \cdot u_{\top}^0 + \sin(\omega_0 t) \cdot u_{\perp}^0) \\ &= M_{\top} \cdot \mathrm{Re}((u_{\top}^0 - i \cdot u_{\perp}^0) \cdot \mathrm{e}^{i\omega_0 t}) \end{aligned} \tag{10}$$

3. The proton magnetic resonance sounding

From the previous section, it follows that as a result of an excitation pulse of moment $q = I \cdot \tau$ (product of the current intensity I by the pulse duration τ) within a transmitter (Tx) antenna, each small volume $\mathrm{d}V(p)$ of the subsurface centred at point p generates a relaxation electromagnetic field which is that of a rotating magnetic dipole of moment $\mathrm{d}M(p)$ that is perpendicular to the local static magnetic field and whose initial intensity is given by

$$\mathrm{d}M(p)\,|_{t=0} = M_0 \cdot w(p) \cdot \sin\left(\frac{1}{2}\gamma \cdot b_{\perp}^{\mathrm{Tx}}(p) \cdot q\right) \cdot \mathrm{d}V(p) \tag{11}$$

where $w(p)$ is the water content distribution, M_0 is the magnetic moment of protons and γ is the gyromagnetic ratio as defined above, and $b_{\perp}^{\mathrm{Tx}}$ is the component of the energising magnetic induction field (for a unit current in the transmitter loop) perpendicular to the static magnetic induction field $\boldsymbol{B}_0$. Since the measurable effect is linked to the transverse magnetisation, the decay time constant of the observed relaxation is the transverse relaxation one,

T_2; however, because of natural inhomogeneities in the geomagnetic field magnitude due to a nonzero magnetic susceptibility of rocks, the observed decay time constant is somewhat a shorter one, $T_2^* \leq T_2$.

Since we are using $e^{i\omega_0 t}$ time dependence, the signal induced in the receiver (Rx) antenna (Fig. 4) is equal to $-i\omega_0$ times the sum of the flux of all the relaxation magnetic dipoles. Using the reciprocity theorem, this induced voltage is thus

$$E(t) = -\int_V \omega_0 M_0 \cdot w(p) \cdot b_\perp^{\mathrm{Rx}}(p) \cdot \sin\left(\frac{1}{2}\gamma \cdot b_\perp^{\mathrm{Tx}}(p) \cdot q\right) e^{-t/T_2^*(p)} \cdot \mathrm{d}V(p) \quad (12)$$

where $b_\perp^{\mathrm{Rx}} = \langle i \cdot \boldsymbol{b}^{\mathrm{Rx}}, u_\top^0 - i \cdot u_\perp^0 \rangle = \langle \boldsymbol{b}^{\mathrm{Rx}}, u_\top^0 + i \cdot u_\perp^0 \rangle$, $\boldsymbol{b}^{\mathrm{Rx}}$ being the (virtual) magnetic induction field that would be created by a unit current in the receiver antenna. If the receiver antenna is the same as the transmitter antenna, then $b_\perp^{\mathrm{Rx}} = b_\perp^{\mathrm{Tx}}$ and the received signal will be in-phase with the transmitted pulse. However, if the receiver antenna is separate from the transmitter antenna, in most locations, $\boldsymbol{b}^{\mathrm{Rx}}$ will have a nonzero component along $u_\top^0$ so that there will be some out-of-phase contribution.

Eq. (12) is the basic equation for proton magnetic resonance sounding. It includes known variables:

- the angular Larmor frequency ω_0 and the nuclear magnetisation M_0 for protons that are derived from the magnitude of the geomagnetic field, the latter being usually measured with a proton magnetometer;
- the electromagnetic field components $b_\perp^{\mathrm{Tx}}$ and $b_\perp^{\mathrm{Rx}}$ that can be numerically computed once the geometry of the transmitting and receiving antennas is known;
- the magnetic resonance signal $E(t)$ that is measured with an appropriate proton magnetic resonance instrument;

and unknown variables, the water content $w(p)$ and the transverse relaxation time constant $T_2^*(p)$ that are the parameters of the subsurface to be obtained by inversion of the field measurements $E(t)$. For a given q, $E(t)$ is linear with regard to $w(p)$. The q dependence is nonlinear through the sine function but can be computed numerically. For each q value, the maximum signal contribution will come from a definite depth range, as shown later on: this opens the possibility of depth sounding, the parameters of the subsurface being determined then by solving an inverse problem.

Since the field set-up for proton magnetic resonance measurements generally makes use of a coincident transmitter and receiver loop antenna, we will use this configuration hereafter.

3.1. A coincident transmitter and receiver circular loop above a resistive half-space

The electromagnetic field of a circular loop of finite radius a can be expressed in terms of elliptic integrals (Keller and Frischknecht, 1966; Kaufman and Keller, 1983). Using the composite parameter

$$m(a,r,z) = \sqrt{\frac{4ar}{(a+r)^2 + z^2}}, \quad (13)$$

the radial and vertical components of the magnetic induction field are:

$$b_r(a,r,z) = \frac{\mu}{2\pi \cdot \sqrt{(a+r)^2 + z^2}} \cdot \left[\frac{2 \cdot a \cdot z}{(a-r)^2 + z^2} \cdot E(m(a,r,z)) - \frac{4 \cdot a \cdot z}{(a+r)^2 + z^2} \cdot D(m(a,r,z))\right] \quad (14a)$$

$$b_z(a,r,z) = \frac{\mu}{2\pi \cdot \sqrt{(a+r)^2 + z^2}} \cdot \left[\frac{a^2 - r^2 - z^2}{(a-r)^2 + z^2} \cdot E(m(a,r,z)) + K(m(a,r,z))\right] \quad (14b)$$

where $K(m) = \int_0^{\frac{\pi}{2}} \frac{1}{\sqrt{1 - m^2 \cdot \sin(\psi)^2}} \cdot \mathrm{d}\psi$ and $E(m) = \int_0^{\frac{\pi}{2}} \sqrt{1 - m^2 \cdot \sin(\psi)^2} \cdot \mathrm{d}\psi$ are the complete elliptic

integrals of the first and second kind, and $D(m) = \frac{K(m)-E(m)}{m^2} = \int_0^{\frac{\pi}{2}} \frac{\sin(\psi)^2}{\sqrt{1-m^2\cdot\sin(\psi)^2}} \cdot d\psi$.

Using the above formulas, it is possible to compute the response $E_d(q)$ of thin water layers at various depths. The results are plotted in Figs. 5–7 for three values of the Earth's magnetic field inclination (90°, 45°, and 0°).

It should be noted that the lower amplitude responses observed at lower latitudes are due to the lower magnitude of the Earth's magnetic field since the responses are proportional to the square of this magnitude.

3.2. Measured water content

If V is a given volume within the subsurface, V_W the part of it filled with water, and V_R the part of it made of dry rocks (or empty pores), we can write $V = V_W + V_R$. The water part V_W can be subdivided

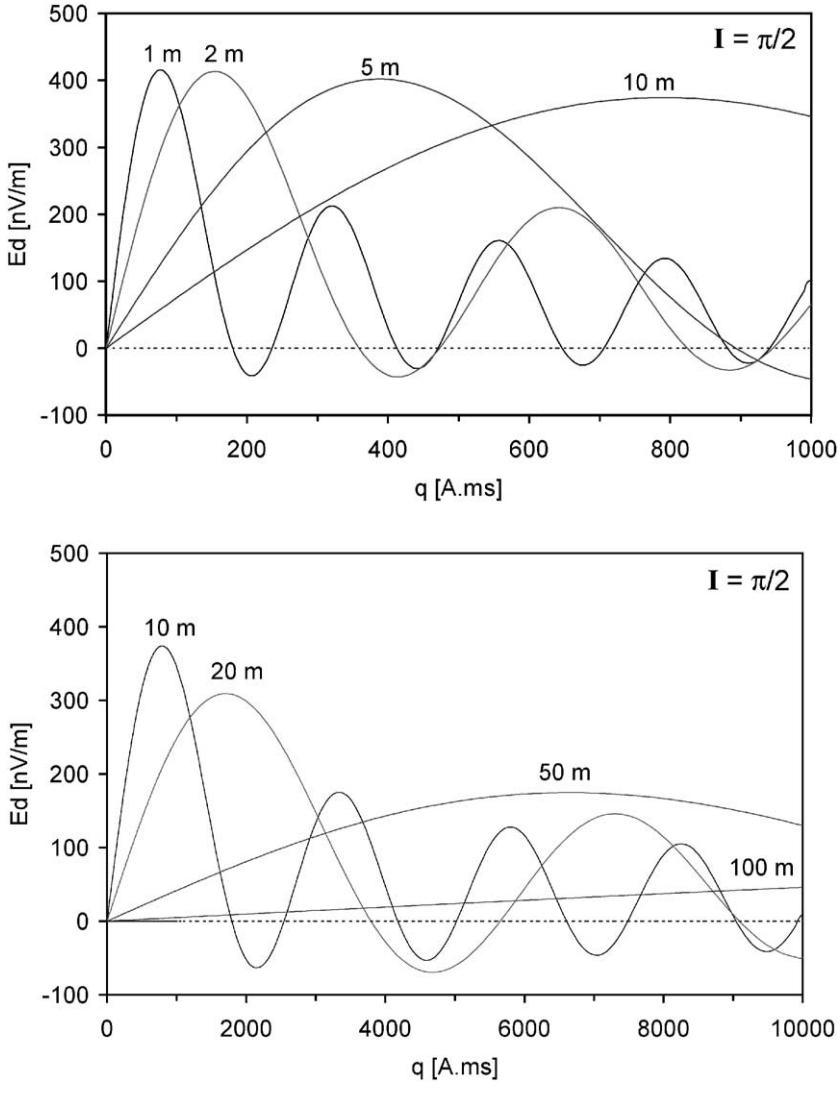

Fig. 5. Thin layer response for a circular loop (100 m in diameter) over a resistive Earth at a 90° magnetic inclination (60,000 nT magnetic field); the upper plot is for smaller depths and small pulse moments, while the lower plot is for larger depths and larger pulse moments.

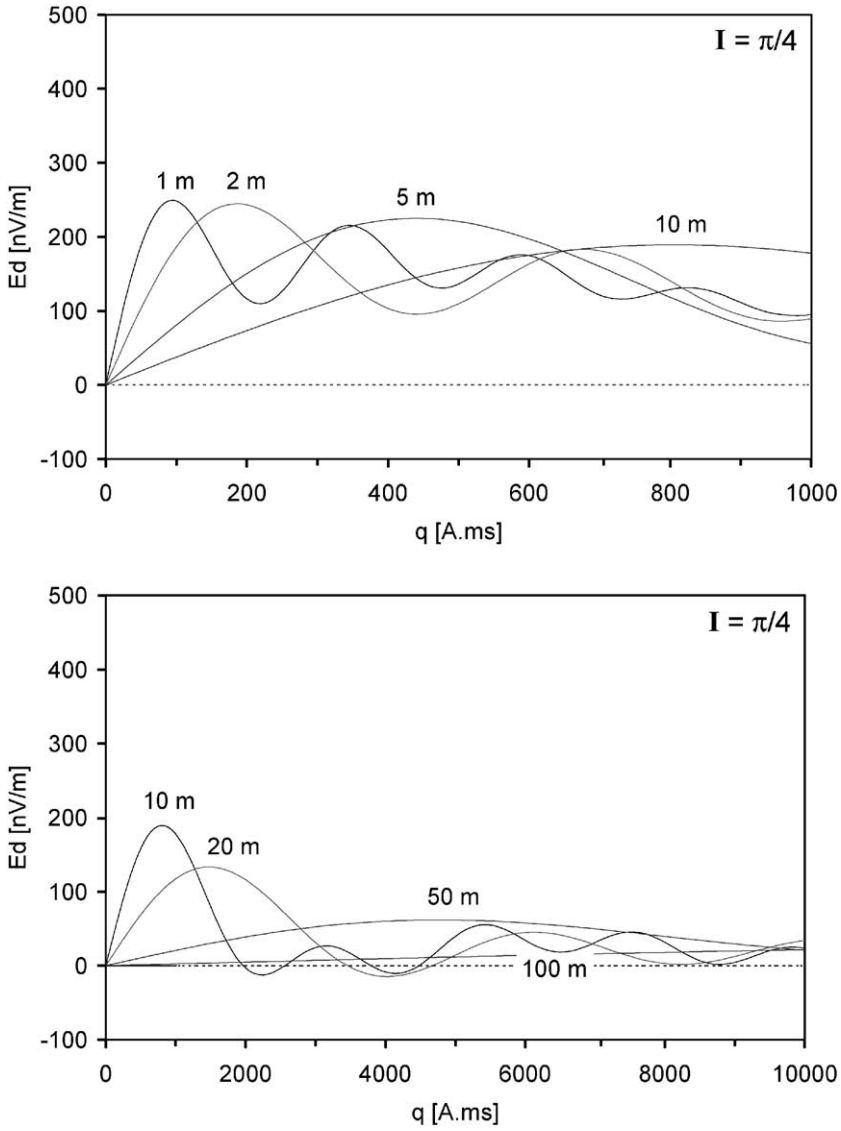

Fig. 6. Thin layer response for a circular loop (100 m in diameter) over a resistive Earth at a 45° magnetic inclination (37,950 nT magnetic field); the upper plot is for smaller depths and small pulse moments, while the lower plot is for larger depths and larger pulse moments.

into two parts: free water V_F (water, which is unbounded to grain walls and can be extracted from the rock) and bounded water V_B. Thus, we will assume that $V_W = V_F + V_B$. These two parts of subsurface water are differentiated by a fundamental difference in the decay time between the magnetic resonance responses from free water and that from bounded water: the decay time of the signal generated by the latter is much shorter than that generated by the former.

Although further research is still required to establish a precise relationship between the decay times of the magnetic resonance signal and the parameters of groundwater in a porous medium or a fractured rock, field experiments show that the decay time for bounded water is less than 20–30 ms and that for

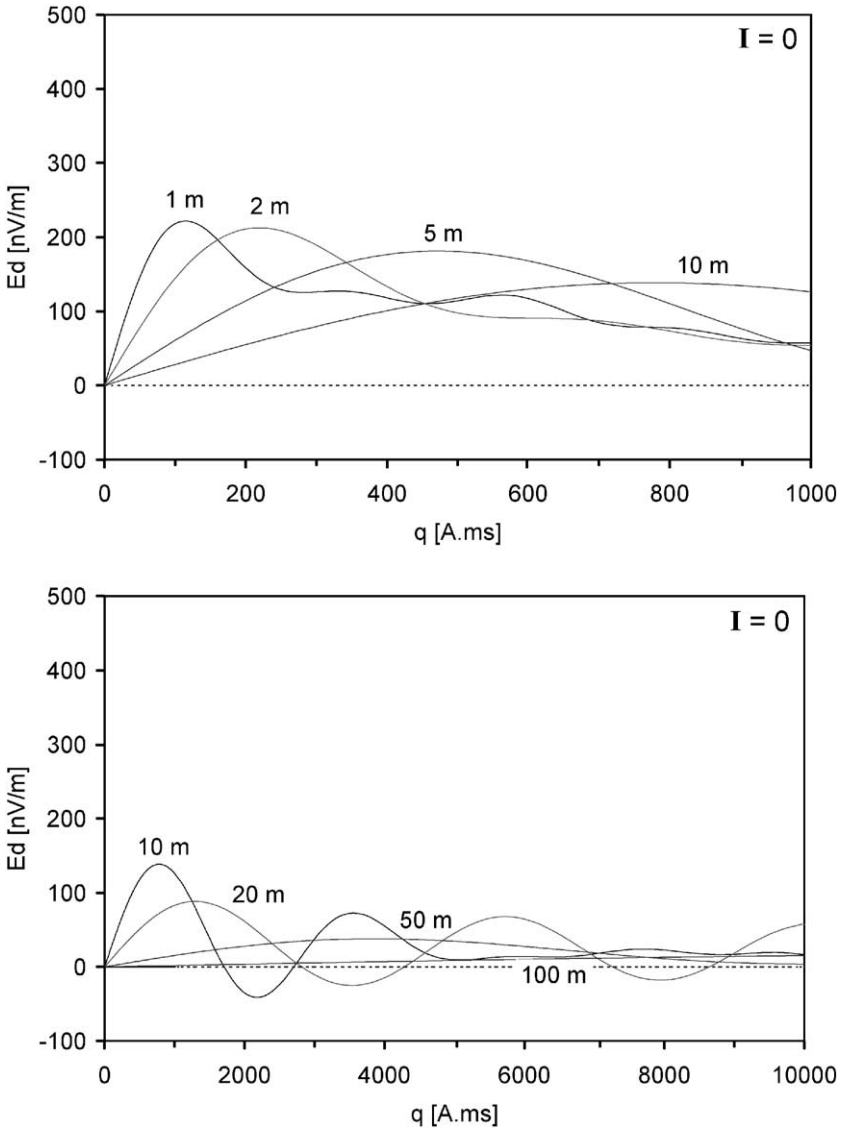

Fig. 7. Thin layer response for a circular loop (100 m in diameter) over a resistive Earth at a 0° magnetic inclination (30,000 nT magnetic field); the upper plot is for smaller depths and small pulse moments, while the lower plot is for larger depths and larger pulse moments.

free water is between 30 and 1000 ms (Schirov et al., 1991). As currently available, proton magnetic resonance equipment such as Hydroscope (ICKC, Russia) and NUMIS (IRIS-Instruments, France) do not permit measurements of very short signals (less then 30 ms), we may say that only the signals from the free water (V_F) are measured. Hence, the water content measured is the part of the total volume of the subsurface occupied by the free water, i.e. $w = V_F/V$.

3.3. Relationship between the transverse relaxation time and the mean size of pores

The transverse relaxation time T_2^* that is obtained with standard proton magnetic resonance measurements describes the spin–spin interaction. It is the characteristic time for the loss of coherency in the spin rotation and is linked to the mean size of the water-filled pores through two complementary phenomena.

(a) As the magnetic susceptibility χ_R of the rock matrix is usually nonzero (or more pointedly, different from the water) and as some remnant magnetisation may also occur, magnetic field gradients will be generated at the pore boundary (rock grain walls); such gradients are roughly proportional to χ_R/r^3, where r is the distance from the grain wall and will lead to differences in the Larmor frequencies so that the spin rotation will loose its phase coherency more quickly for water molecules close to the boundary; this will shorten the decay time in a stronger way for small pores than for larger ones.

(b) As a result of the diffusion of water molecule within the pore space, such molecules will bump into the pore boundary and acquire a new arbitrary magnetic moment orientation; intuitively, the resulting decay time constant should be proportional to the characteristic dimension of the pore; for porous media, the following relationship has been derived for either the longitudinal or transverse decay time:

$$\frac{1}{T} = \frac{1}{T_{\text{bulk}}} + \rho \cdot \frac{S_{\text{pore}}}{V_{\text{pore}}} \tag{15}$$

where the second term in the right-hand side involves the surface area to volume ratio of a pore and a surface relaxivity factor; the bulk water decay time is linked to the magnetic field inhomogeneity created by the magnetic moment of every proton.

We should recall here that according to Eq. (12), only an integral signal from the subsurface water can be measured from the surface, and hence, the measured decay time T_2^* is also an integral characteristic. When most of the water volume is located in the nonperturbed geomagnetic field (in open pores far away from grain walls), the measured magnetic resonance signal will decay with a time constant close to that of the bulk water: $T_2^* \cong T_{\text{bulk}}$. When most of the water volume is located in an inhomogeneous geomagnetic field (close to grains), the signal will decay with a much shorter time constant: $T_2^* < T_{\text{bulk}}$. Typical values are $T_2^* > 300$ ms for water in gravel or coarse sand, and $T_2^* < 50$ ms for water in sandy clay (Schirov et al., 1991).

The relationship between the measured relaxation time T_2^* and pore geometry in an aquifer is the physical basis for establishing a relationship between the hydrogeological parameters and proton magnetic resonance ones. However, one should keep in mind that any such relationship will depend on the magnetic susceptibility of rocks that may significantly vary from one site to another. Also, the thickness of the bounded water layer around rock particles will depend on the mineralogy that may vary quite independently from one type of rock to the other. Hence, no universal relationship is to be expected and some regional calibration is mandatory.

4. Signal processing

As stated previously, the actual Larmor frequency will slightly vary from one place to another. Also, there could be some phase shift in the signals, for instance, in an electrically conductive medium. Hence, for a given value of the energising pulse parameter q, the measured magnetic resonance response should be expressed as the sum of exponentially decaying oscillating signals

$$E(t) = \int_V E_0(p,q) \cdot \cos(\omega_0(p) \cdot t + \varphi_0(p)) \cdot e^{-t/T_2^*(p)} \cdot \mathrm{d}V(p) + N(t) \tag{16}$$

where $E_0(p,q)$, $T_2^*(p)$, $\omega_0(p)$, and $\varphi_0(p)$ are the initial amplitude, decay time, pulsation, and phase of the signal contribution from volume $\mathrm{d}V(p)$, and $N(t)$ is some additive measurement noise.

For measuring such type of signals, a synchronous detection is usually used (Farrar and Becker, 1971). Using a two-channel detector with a reference angular frequency $\omega_d = 2\pi \cdot f_d$, two signals (in-phase and out-of-phase) are obtained:

$$X(t) = \int_V E_0(p,q) \cdot \cos((\omega_0(p) - \omega_d) \cdot t + \varphi_0(p)) \cdot e^{-t/T_2^*(p)} \cdot \mathrm{d}V(p) + N_X(t), \tag{17a}$$

$$Y(t) = \int_V E_0(p,q) \cdot \sin((\omega_0(p) - \omega_d) \cdot t + \varphi_0(p)) \cdot e^{-t/T_2^*(p)} \cdot \mathrm{d}V(p) + N_Y(t). \tag{17b}$$

As the reference angular frequency of the detector ω_d is selected to be as close as possible to the Larmor

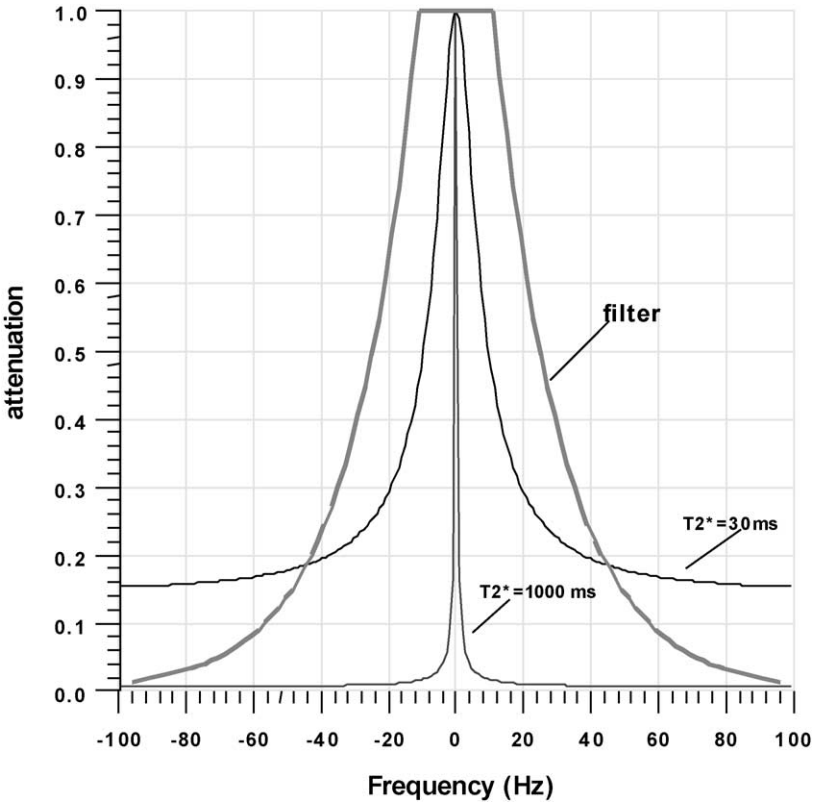

Fig. 8. Characteristics of a low-pass filter to be applied to proton magnetic resonance signals after synchronous detection.

frequency and as the variation of the Larmor frequency in the investigated volume is usually no more than a few hertz, we can usually assume $\max_v(\omega_0(p) - \omega_d) < 5$ Hz, so that the synchronous detector will provide low-frequency signals. A low-pass filter is then applied: its band width (around zero) should be selected as narrow as possible but still should not distort the signal. In Fig. 8, the spectrum of the longest ($T_2^* = 1000$ ms) and the shortest ($T_2^* = 30$ ms) signals is depicted, together with a suitable low-pass filter. Because of possible variations in the Larmor frequency, a flat zone on the filter response is needed. In some cases, when only long signals are of interest, a narrower filter may be selected.

As the proton magnetic resonance response is usually very small in comparison with both the cultural and natural electromagnetic noises, even a very narrow filter does not allow getting a good enough signal-to-noise ratio (S/N). In order to improve the signal-to-noise ratio, a stacking procedure must also be used. It consists of averaging up records: $E(t) = \sum_{i=1}^{n} E_i(t)/n$. In the case of non-correlated noise, the signal-to-noise ratio is increased $\sqrt{n}$ times after n stacks.

A more effective stacking scheme, namely weighted stacking, can be applied if the noise magnitude is not statistically constant during the data acquisition time (non-white noise). Such a scheme is based on a noise estimate s_i defined as

$$s_i^2 = \frac{1}{\Delta T}\int_0^{\Delta T} (X_i(t)^2 + Y_i(t)^2) \cdot \mathrm{d}t, \tag{18}$$

ΔT being the observation window. Each record is assigned the weight $\eta_i = 1/s_i^2$, and records are averaged up with such weights:

$$E(t) = \sum_{i=1}^{n} \eta_i E_i(t) / \sum_{i=1}^{n} \eta_i. \tag{19}$$

After stacking and filtering, the parameters of the resulting magnetic resonance signal are determined as a function of the energising pulse moment q:

- initial amplitude $E_0(q)$
- average decay time constant $T_2^*(q)$
- frequency shift (difference between reference frequency and average Larmor frequency) $\omega_0(q)$
- and phase shift $\varphi_0(q)$.

For this purpose, a signal-processing algorithm based on nonlinear fitting can be applied (Legchenko and Valla, 1998).

The initial amplitude $E_0(q)$ and the decay time constant $T_2^*(q)$ are used in the inversion to obtain the water content $w(z)$ and the decay time $T_2^*(z)$ depth distributions. The frequency shift $\omega_0(q)$ is used for estimating the inhomogeneity of the geomagnetic field. The phase shift $\varphi_0(q)$ is mostly related to the electrical conductivity of rocks.

5. Data inversion method

For the inversion of proton magnetic resonance data, a variety of schemes may be used (Guillen and Legchenko, 1997, 1998). However, it is still the Tikhonov regularisation method (Legchenko and Shushakov, 1998) that is used in standard software provided with commercially available equipment such as the NUMIS system from IRIS-Instruments.

We will first consider the inversion of the initial amplitude $E_0(q)$ that leads to the water content distribution. Assuming a horizontally stratified hydrogeological model, Eq. (12) applied to the initial signal amplitude ($t=0$) can be simplified to a Fredholm linear integral equation of the first kind

$$E_0(q) = \int_0^\infty K(q,z) \cdot w(z) \cdot \mathrm{d}z, \tag{20}$$

where $K(q,z) = \omega_0 M_0 \int_{x,y} b_\perp^{\mathrm{Rx}} \sin\left(\frac{1}{2}\gamma b_\perp^{\mathrm{Tx}} q\right) \cdot \mathrm{d}x\mathrm{d}y$. Note that $K(q,z)$ is the response of a thin water layer, the same as $E_\mathrm{d}(q)$ in Section 3.1. Numerical results show that the distant protons produce a negligibly small signal, so that it is enough to perform the x,y integration in a circle of diameter $2D$ (D being the antenna diameter) and the z integration down to a distance L equal to D.

The vertical distribution of water content $w(z)$ is the solution of Eq. (20). An approximate solution may be obtained by projecting this equation onto a finite-dimensional subspace and solving the projected equation

$$\sum_j \kappa_j(q_i) \cdot w_j = E_{0,i} \tag{21}$$

where $i=1,2,\ldots,I$ is the running index for the performed measurements (I being the number of q values), $j=1,2,\ldots,J$ is the running index for the projection subspace, and $\kappa_j(q)$ is a set of kernel vectors obtained by projecting the kernel $K(q,z)$ on a set of basis functions $\beta_j(z)$, so that

$$w(z) = \sum_j w_j \beta_j(z), \quad \text{and} \quad \kappa_j(q) = \int_0^\infty K(q,z)\beta_j(z)\mathrm{d}z. \tag{22}$$

In the problem considered here, the basis functions may be taken as boxcar functions. Hence, the kernel vectors are the elementary responses from the layers of water ($w_j=1$), characterised by their depth z and thickness Δz. When the depth intervals are $0 \le z \le L$, $\Delta z_j = z_{j+1} - z_j$, $L = \sum_{j=1}^{J} \Delta z_j$, the basis functions are $\beta_j(z_j \le z < z_{j+1}) = 1$, $\beta_j(z < z_j,\ z \ge z_{j+1}) = 0$, and the kernel vectors are $\kappa_j(q) = \int_{z_j}^{z_{j+1}} K(q,z)\mathrm{d}z$.

In a matrix notation, the projected equation can be written as

$$\boldsymbol{A} \cdot \boldsymbol{w} = \boldsymbol{e}_0, \tag{23}$$

where $\boldsymbol{A} = [a_{i,j}]$ is an $I \times J$ rectangular matrix with elements $a_{i,j} = \kappa_j(q_j)$, $\boldsymbol{e}_0 = (E_{0,1}, E_{0,2}, \ldots, E_{0,i}, \ldots, E_{0,I})^{\mathrm{T}}$, $E_{0,i} = E_0(q_i)$ is the set of experimental data, and $\boldsymbol{w} = (w_1, w_2, \ldots, w_j, \ldots, w_J)^{\mathrm{T}}$, $w_\mathrm{j} = w(\Delta z_j)$ is the vertical distribution of water content, the symbol T denoting transposition.

The inversion is carried out according to the well-known Tikhonov regularisation method (Tikhonov and Arsenin, 1977) through the minimisation of the Tikhonov functional

$$M_\eta(w) = \| \boldsymbol{A} \cdot \boldsymbol{W}_\eta - \boldsymbol{e}_0 \|_{L_2} + \eta \cdot \| \boldsymbol{W}_\eta \|_{L_2}, \tag{24}$$

where $\boldsymbol{W}_\eta$ is the solution vector that minimises the Tikhonov functional ($\boldsymbol{M}_\eta$) for a given parameter of regularisation $\eta>0$.

To solve this minimisation problem, the discrepancy principle introduced by Morozov (1966) is applied. It is based on the fact that for erroneous data, it does not make much sense to have the residual $\|\boldsymbol{A}\cdot\boldsymbol{W}_\eta-\boldsymbol{e}_0\|_{L_2}$ smaller than the experimental error. Hence, for a given noise level estimate $\varepsilon>0$, we need to find a solution with a residual $\|\boldsymbol{A}\cdot\boldsymbol{W}_\eta-\boldsymbol{e}_0\|_{L_2}\le\varepsilon$ and stabilise it by making $\|\boldsymbol{W}_\eta\|_{L_2}$ small. $\boldsymbol{W}_\eta$ is an approximation of the solution of matrix Eq. (23). When $\varepsilon\to 0$, $\eta(\varepsilon)\to 0$, and $\boldsymbol{W}_\eta$ tends to $\boldsymbol{W}$, the projection of the actual water distribution. For the optimisation itself, the conjugate gradient method (Stoer and Bulirsch, 1980) is used.

In order to get the decay time distribution $T_2^*(z)$, we assume that in Eq. (12), the small finite volume $\mathrm{d}V(p)$ is homogeneous with regard to both the water content and decay time. It means that while the initial amplitude of the signal generated by this volume is a function of the pulse parameter q, the decay time $T_2^*(q)$ is independent of q. Thus, instead of fitting time series $E(t,q)$ by an exponential function for each q for deriving the $T_2^*(q)$ values that could be inverted into $T_2^*(z)$, we first invert $E(t,q)$ into $w(t,z)$ and then fit each of the latter by an exponential function, thus providing the $T_2^*(z)$ values. For the inversion of $E(t,q)$

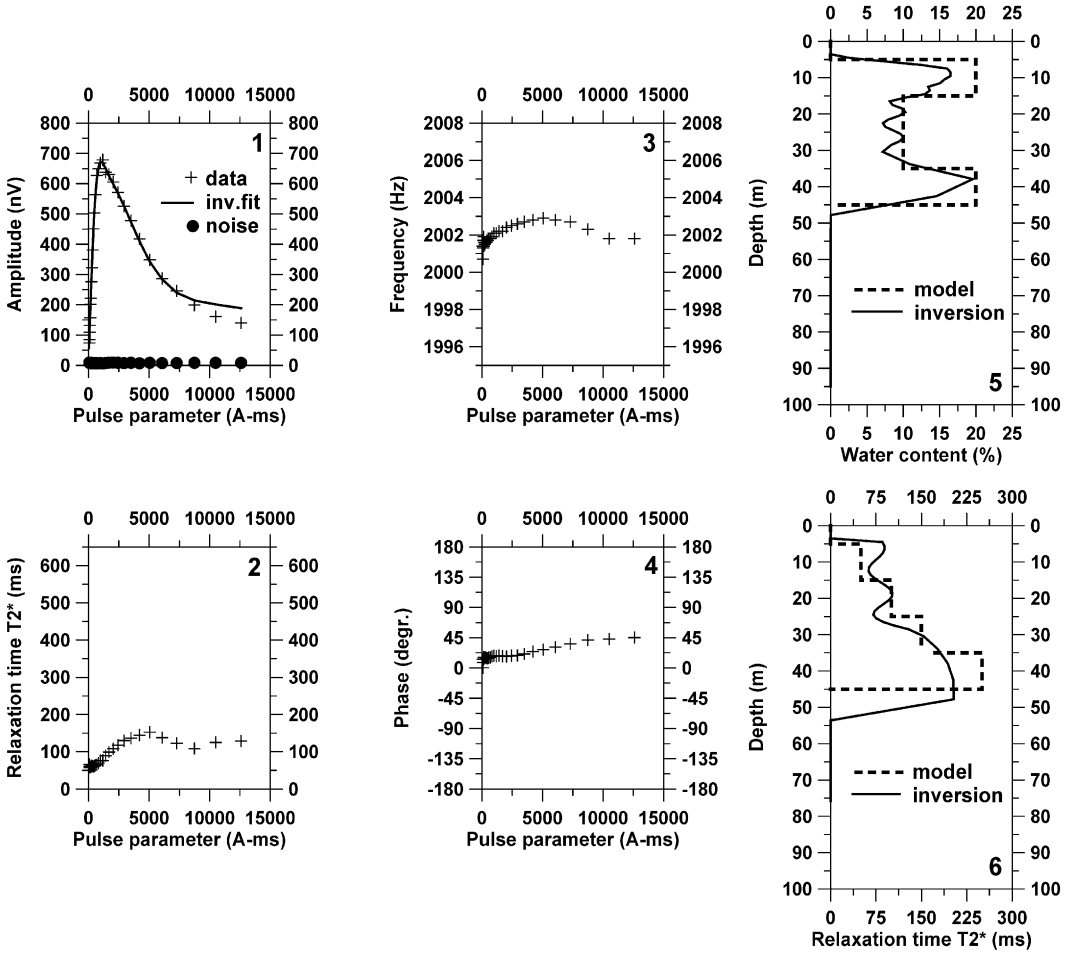

Fig. 9. Results of inversion of the synthetic data with 40 nV random noise added.

data, the same algorithm as for the inversion of $E_0(q)$ is used.

5.1. Example of synthetic data processing

For demonstrating the effectiveness of the above-presented processing schemes, we will use the following model:

- the transmitting/receiving antenna is a circular loop of 100 m in diameter,
- the inclination of the geomagnetic field is 60°,
- the electrical resistivity is 50 Ω m from 0 to 30 m and 5 Ω m from 30 to 100 m,
- the water distribution is made of four layers listed in the following table:

Depth		Water content (%)	Decay time (ms)	Larmor frequency (Hz)
From (m)	To (m)			
5	15	20	50	2000
15	25	10	100	2001
25	35	10	150	2002
35	45	20	250	2003

- a random noise of 40 (model 1) and 400 nV (model 2) is added to the signal.

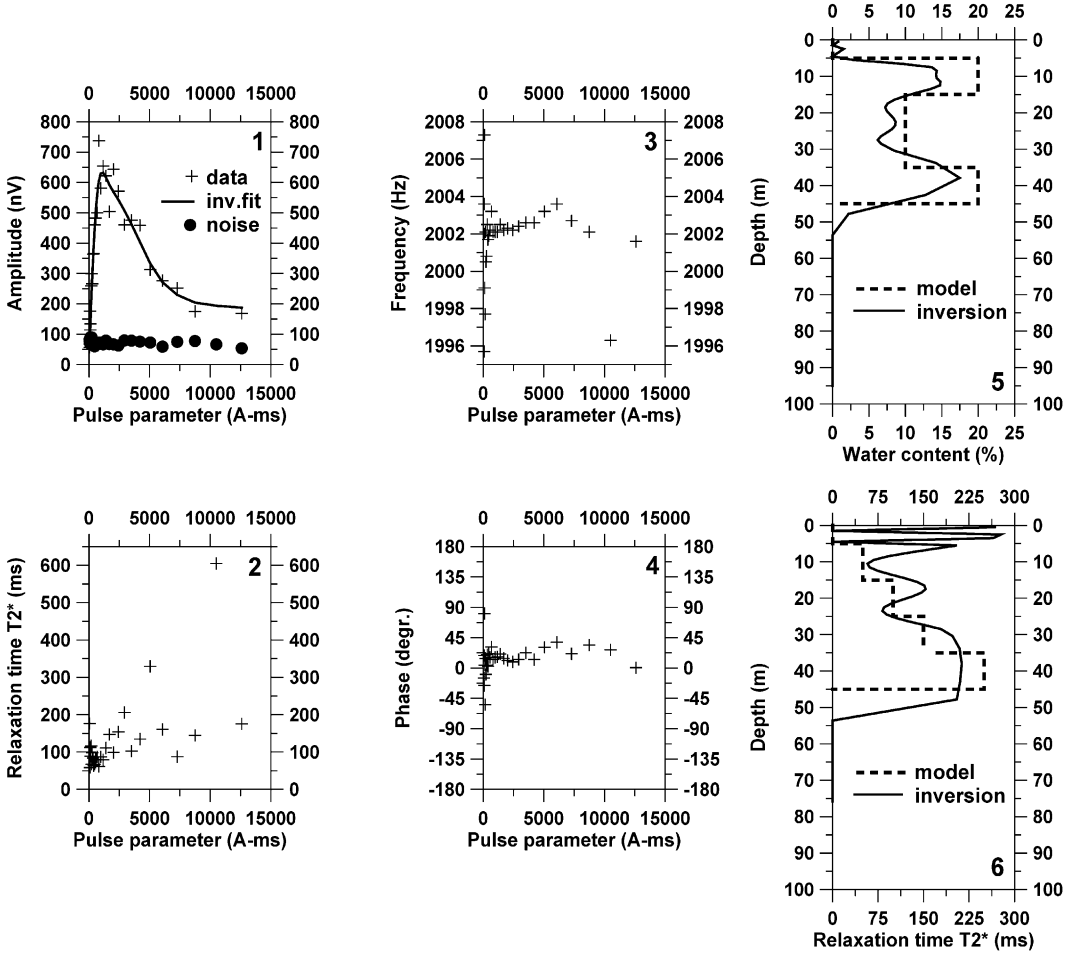

Fig. 10. Results of inversion of the synthetic data with 400 nV random noise added.

Synthetic data were inverted with the standard NUMIS interpretation software implemented as presented above. Results are presented in Fig. 9 (model 1) and Fig. 10 (model 2). Each figure consists of six graphs:

1. Measured amplitude of the signal vs. the pulse moment $E_b(q)$ extrapolated in the beginning of the registration window, reconstructed theoretical signal after inversion, and noise level,
2. Measured relaxation time of the signal decay vs. the pulse moment: $T_2^*(q)$,
3. Measured frequency of the signal vs. the pulse moment,
4. Measured phase of the signal vs. the pulse moment: $\varphi_0(q)$,
5. Water content $w(z)$ vs. depth,
6. Decay time $T_2^*(z)$ vs. depth.

The following comments can be made for the graphs in Fig. 9.

- The measured frequency (Graph 3) of the response is varying smoothly around the reference frequency of the synchronous detector, depending on the signal contribution of the various layers that are located in an inhomogeneous geomagnetic field.
- The phase (Graph 4) of the signal also varies smoothly as the pulse moment increases; such phase

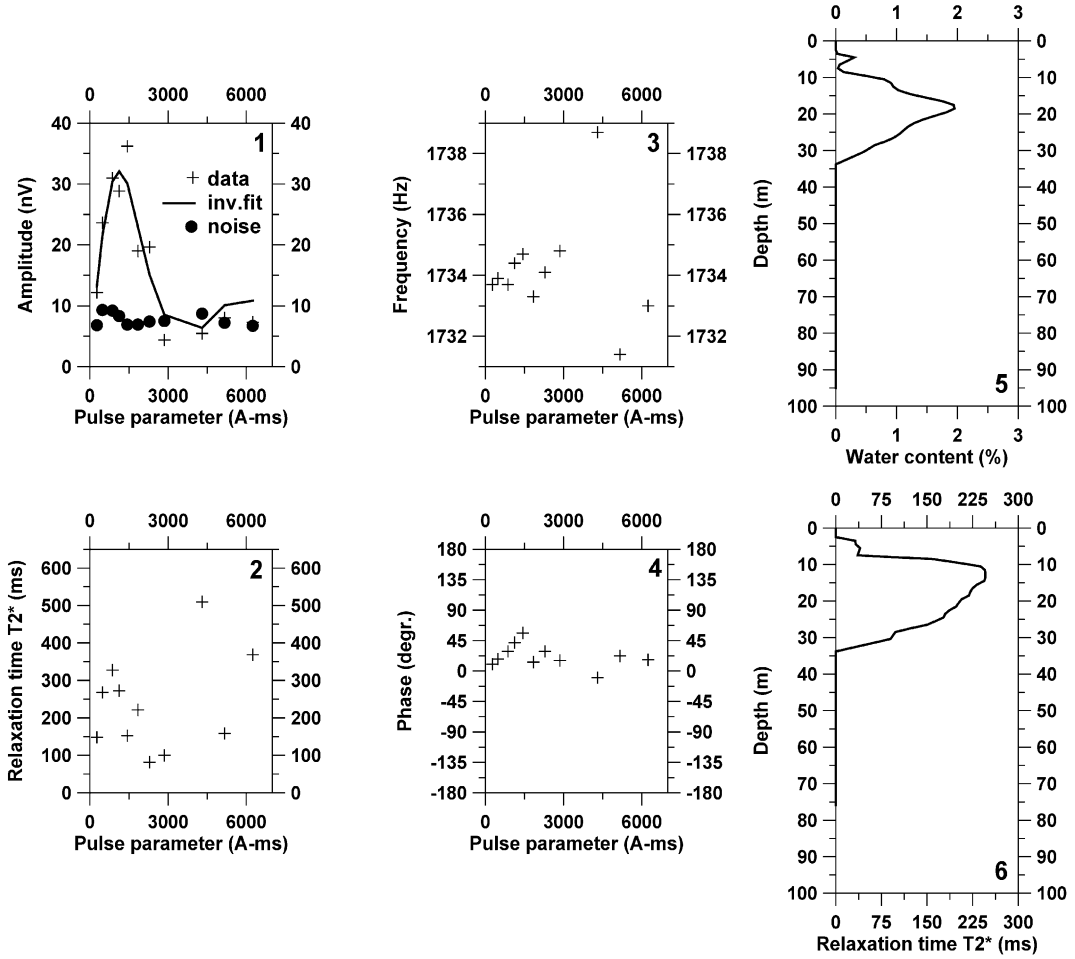

Fig. 11. Results of a proton magnetic resonance sounding performed in Saudi Arabia.

variations originate from electrically conductive layers in the subsurface; this, together with the smooth variation of the measured frequency, is a reliable indication that the signal is indeed a proton magnetic resonance response from the underground water. If, on the other hand, the frequency and/or the phase were varying quite randomly, it would mean that some other electromagnetic signal has been measured, and in such case, the data should be treated with more caution.

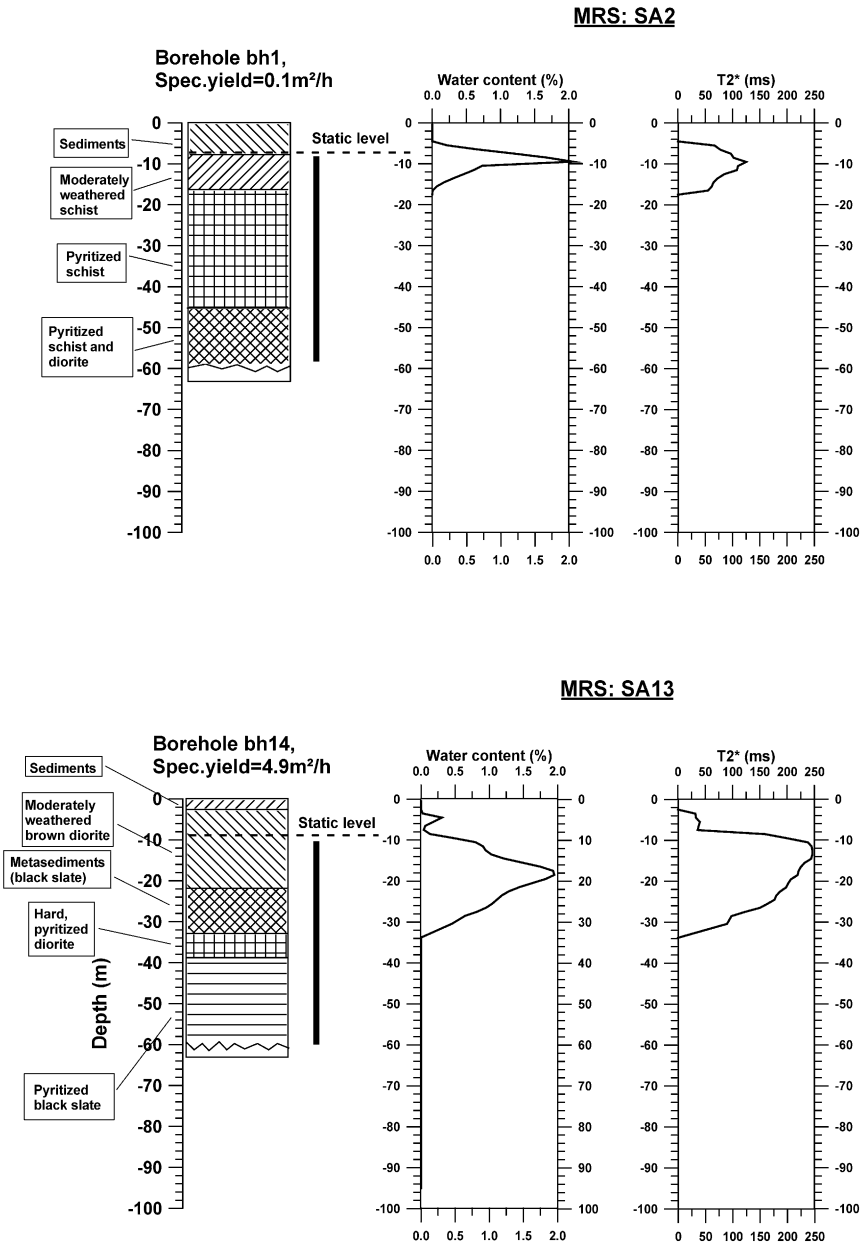

Fig. 12. Comparison of magnetic resonance interpretation and drilling results in Saudi Arabia.

• Variations in the decay time (Graph 2) are also observed here depending on the signal contribution of the various layers having different intrinsic decay times.

• The signal-to-noise ratio (S/N) is good and a close fit between the measured data and synthetic responses is obtained by the inversion (Graphs 1 and 5), so that the inversion results can be considered quite reliable.

• Two main aquifers (5–15 and 35–45 m) are detected; the water content in the shallow aquifer is about 16% and that in the deep aquifer is about 19%; these two aquifers are separated by a layer with a smaller amount of water in it (about 8%). The decay time is about 70 ms at the top and is increasing to about 205 ms rather smoothly with increasing depth. Interpreting $T_2^*(z)$ results, one should be aware that the decay time measurements are meaningful only for depth interval with nonzero water content.

Comparing the model with what was derived from the data, one gets an idea about the accuracy of the proton magnetic resonance results that could be obtained in good conditions of measurements, but over a quite complicated structure. The layers with the highest water contents are quite well-identified although their boundaries with the intermediate layers are not so well resolved. The variations in the decay times are also recovered.

When 400 nV of random noise is added to the model (Fig. 10), the noise level after filtering is about 80 nV ($S/N \cong 5-10$). Despite such noise, a fair coherency in the various curves can be observed and the obtained results still correspond rather well to the model, except for somewhat noisier decay time estimates.

5.2. A field example

As an example of a proton magnetic resonance sounding, we will use field results of a survey performed in Saudi Arabia (Legchenko et al., 1998). During this survey, proton magnetic resonance soundings were carried out along a few profiles over subsurface anomalies detected by electromagnetic measurements. A number of boreholes were also drilled in this area. For the fieldwork, a NUMIS system with a 100-m-diameter circular antenna was used.

The results of the proton magnetic resonance sounding at site "SA13" are shown in Fig. 11. The maximum signal was found to be less than 40 nV but the measured frequency and the phase of the signal are rather coherent for pulses with relaxation signal amplitude above the noise level. Hence, a magnetic resonance signal was indeed detected. From the inversion, a water-bearing zone is found between 5 and 30 m. The decay time is short in the shallow part of this zone. It could be interpreted as a transitional area between the vadose zone (with capillary water) and the water saturated zone (aquifer below the water table). The decay time and the water content then increase with increasing depth. In hard-rock environments, such a water-bearing zone usually corresponds to a water-saturated weathered zone (Palacky et al., 1981).

Fig. 12 shows the comparison between the proton magnetic resonance sounding results and two corresponding borehole data. The water table measured in the borehole corresponds to the depth at which a 50-ms decay time is reached. Hence, water layers with smaller decay times above should indeed be non-saturated ones. Generally, the aquifers revealed by the proton magnetic resonance measurements correspond well to the weathered zone identified from the boreholes. Quite naturally, the thicker aquifer detected by "SA13" sounding corresponds to a larger yield of the corresponding borehole BH14.

These results illustrate the information that can be provided by proton magnetic resonance measurements and may serve for the best positioning of water-supply boreholes and for water resources evaluation.

6. Conclusions

The theoretical basis and numerical modelling of proton magnetic resonance measurements, together with the data acquisition, signal processing, and interpretation techniques have been presented. The use of the corresponding numerical schemes has been demonstrated for both the synthetic and field data. The current state-of-the-art methods offer numerous possibilities for one-dimensional applications in hydrogeological investigations. Various areas are still open for further research and development, such as improved noise reduction strategies in data acquisition and 2D/3D data interpretation: this would further enlarge the application span.

References

Abragam, A., 1961. The Principles of Nuclear Magnetism. Oxford Univ. Press, 648 pp.

Farrar, T.C., Becker, E.D., 1971. Pulse and Fourier Transform NMR. Academic Press, New York.

Guillen, A., Legchenko, A.V., 1997. Inverse Problem of Magnetic Resonance Measurements Applied to Water Resource Characterization. Expanded Abstracts, SEG'97, Dallas (USA), November 2–7, 1997, vol. I, pp. 446–449.

Guillen, A., Legchenko, A.V., 1998. Inversion of 1D NMR data by the Monte-Carlo method. Proceedings, NMR Imaging of Reservoir Attributes, SEG Summer Research Workshop, August 9–12, 1998, Park City, UT, USA.

Kaufman, A.A., Keller, G.V., 1983. Frequency and Transient Soundings. Elsevier, 620 pp.

Keller, G.V., Frischknecht, F.C., 1966. Electrical Methods in Geophysical Prospecting. Pergamon, Oxford.

Legchenko, A.V., Shushakov, O.A., 1998. Inversion of surface NMR data. Geophysics 63, 75–84.

Legchenko, A.V., Valla, P., 1998. Processing of proton magnetic resonance signals using non-linear fitting. J. Appl. Geophys. 39, 77–83.

Legchenko, A.V., Baltassat, J.M., Beauce, A., Makki, M.A., Al-Gaydi, B.A., 1998. Application of the surface proton magnetic resonance method for the detection of fractured granite aquifers. Proceedings of the IV Meeting of the Environmental and Engineering Geophysical Society (European Section), September 14–17, 1998, Barcelona (Spain), pp. 163–166.

Morozov, V.A., 1966. On the solution of functional equations by the method of regularization. Sov. Math. Dokl. 7, 414–417 (English translation).

Palacky, G.J., Ritsema, I.L., de Jong, S.J., 1981. Electromagnetic prospecting for groundwater in pre-Cambrian terrains in the republic of Upper Volta. Geophys. Prospect., Eur. Assoc. Geosci. Eng. 29, 932–955.

Schirov, M., Legchenko, A., Creer, G., 1991. New direct non-invasive ground water detection technology for Australia. Explor. Geophys. 22, 333–338.

Slichter, C.P., 1990. Principles of Magnetic Resonance, 3rd edn. Springer, Berlin, 655 pp.

Stoer, J., Bulirsch, R., 1980. Introduction to Numerical Analysis. Springer, Berlin.

Tikhonov, A., Arsenin, V., 1977. Solution of Ill-Posed Problems. Wiley.